PASJ: Publ. Astron. Soc. Japan **47**, 551–559 (1995)

Galactic-Center Molecular Arms, Ring, and Expanding Shell. II. Expanding Molecular Shell

Yoshiaki SOFUE
Institute of Astronomy, The University of Tokyo, Mitaka, Tokyo 181
Email sofue@mtk.ioa.s.u-tokyo.ac.jp

(Received 1995 January 14; accepted 1995 August 14)

Abstract

We consider the three-dimensional structure of the so-called 200-pc expanding molecular ring in the Galactic Center by analyzing the $(b, V_{\rm LSR})$ diagrams of the ^{13}CO(J = 1–0) line emission from the Bell-Telephone-Laboratory survey. We show that the (b, V) features can be fitted by a spheroidal shell pinched at the equator (dumbbell-shaped shell), which we call the expanding molecular shell (EMS). The radius is about 180 pc and the vertical extent is more than ±50 pc. The shell is expanding at 160 km s^{-1}, and is rotating at 70 km s^{-1}. The association of the radio continuum emission indicates that the EMS is a mixture of molecular and ionized hydrogen gases. An extended hot (X-ray) plasma appears to fill the interior of the shell. The estimated molecular mass of the shell is $\sim 10^7 M_\odot$ and its kinetic energy $\sim 2 \times 10^{54}$ erg.

Key words: Galaxy: activity — Galaxy: center — Galaxy: kinematics and dynamics — Galaxy: structure — ISM: clouds — ISM: molecules

1. Introduction

The molecular gas in the Galactic Center region is generally confined within a thin dense layer of a few tens of pc thickness comprising the nuclear molecular disk, while a small amount of out-of-plane gas is present, extending up to ∼±50 pc above the disk (see Paper I and the literature cited therein). In Paper I (Sofue 1995) we reanalyzed the longitude-velocity (l, V)diagrams of the ^{13}CO line data of Bally et al. (1987, 1988), and showed the presence of molecular arms and a ring structure within the nuclear disk.

Besides the disk components, the central 200 pc region is characterized by the "200-pc expanding molecular ring," which exhibits high positive- and negative-velocity features consisting of an 'ellipse' in the (l, V) diagram (Scoville 1972: Kaifu et al. 1972, 1974). It has been suggested that this structure is vertically extended for about 100 pc perpendicularly to the galactic plane (Sofue 1989), and might be a part of a cylindrical structure similar to the Galactic Center Lobe (Sofue, Handa 1984). Alternatively, it might be a part of a "parallelogram" in an (l, V) plot (Binney et al. 1991), or this feature might be the inner part of an expanding tilted disk of 2 kpc radius (Liszt, Burton 1978).

In this paper we revisit this prominent feature and investigate its vertical structure based on (b, V) diagrams of the ^{13}CO (J = 1–0) and CS lines observed by Bally et al. (1987) with the Bell Telephone 7-m off-set Cassegrain telescope (BTL survey). The details concerning the data and analysis method are given in Paper I.

2. Dumbbell-Shaped Expanding Molecular Shell

2.1. *Expanding Ring in Longitude-Velocity Diagrams*

The 200-pc expanding molecular ring is recognized in the (l, V) diagrams as high-velocity arcs at $V_{\rm LSR} \sim$ ±150–200 km s^{-1}, which comprises a tilted ellipse (Bally et al. 1978, 1988). It is known that the vertical extent of this feature is as large as ∼ 100 pc (Sofue 1989). The vertical extent is significantly greater than that of the nuclear disk component, which contains 85% of the total emission in the diagram. Since the "expanding" component seen in the (l, V) diagrams amounts to only 15% of the total emission in the central ±1° region, it is not a major disk component. The positive-velocity side of the expanding ring is most clearly visible at $b \sim 4'$, while the negative-velocity side is most clearly seen at $b \sim -15'$. In order to see how the ellipse shows up across its densest parts, we have combined an (l, V) plot at $b = 4'$ for the positive-velocity side and that at $b = -15'$ for the negative-velocity side (figure 1). In the figure the expanding ellipse appears as an almost symmetric feature around the nucleus.

2.2. *Latitude–Velocity (b, V) Diagrams*

In order to investigate the vertical structure of these features, we make use of (b, V) diagrams. Figure 2 shows typical (b, V) plots averaged over 10′ interval of longi-

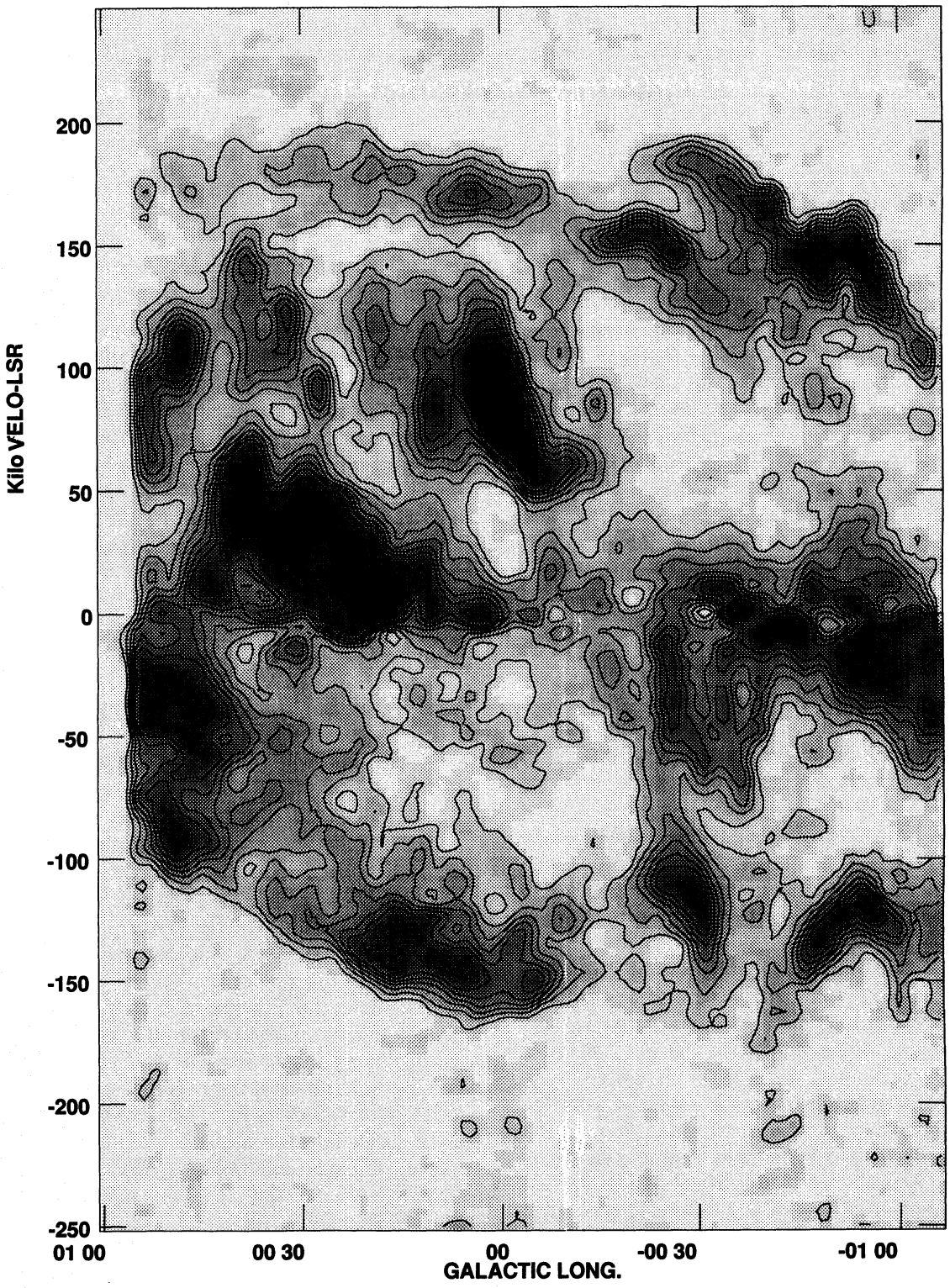

Fig. 1. A composite (l, V) diagram by combining data at $b = +4'$ for the upper half ($V_{\rm LSR} > 0$ km s^{-1}) and that at $b = -15'$ for the lower half ($V_{\rm LSR} < 0$ km s^{-1}). The map has been smoothed by a Gaussian function with a half-width $1' \times 2.7$ km s^{-1}. This diagram shows the expanding ring feature at its clearest part. Contours are in unit of K $T_{\rm A}^*$ at levels $0.1\times$(1, 2, 3, 4, 5, 6, 8, 12, 16, 20, 25). The local and foreground CO emissions have been subtracted by applying the "pressing method" to the BTL cube data (Bally et al. 1987) (see Paper I for the procedure).

tude, where the local components have been subtracted (see Paper I for the analysis). The expanding-ring feature is now recognized as arched features at $V_{\rm LSR} \sim \pm 150$–180 km s^{-1}. These arcs are largely extended in the b direction over $\sim \pm 20'$ (50 pc), and are distinguished from the massive disk component, which has a smaller scale height of $\sim \pm 5$–$10'$. The arcs are all convex with respect to the center of the diagrams. The arcs appear to comprises an ellipse, which is slightly squeezed near the galactic plane, representing a dumbbell-shaped expanding-shell feature in (b, V) space with its neck (equator) at $b = -3'$. This equator coincides with the plane of the major molecular disk crossing Sgr A.

The velocity width of the shell [velocity difference between the positive and negative-most edges of the arcs in the (b, V) plot] appears to vary with longitude. The width attains a maximum at around $l \sim 0°$, and decreases with the distance from the center. Although the present data do not cover the regions at $|l| > 1°$, the decrease in the width indicates that the tangential edges of the expanding shell are located at $l = \pm 1.°2$ (± 180 pc).

Since the higher-velocity part of an expanding feature in a position-velocity plot corresponds to a larger-radius part, the (b, V) ellipse (or dumbbell) features can be most naturally attributed to the cross section of an expanding spheroidal (or dumbbell-shaped) surface (shell), which we call the dumbbell-shaped expanding molecular shell (EMS). From the (l, V) diagrams, the EMS is rotating at about 70 km s^{-1} around the nucleus with the negative-velocity part being at the near-side. This rotation speed is much smaller than the galactic rotation velocity, and may indicate that the gas has been carried from the inner region.

2.3. *Asymmetry about the Galactic Plane, and Anti-correlation with the Disk Component*

The dumbbell-shape in (b, V) space has its equator (neck) at $b = -3'$, which coincides with the plane of the major molecular disk. However, the (b, V) arcs are not symmetric with respect to the equator. The lower-b counterpart is missing at $V_{\rm LSR} > 0$ km s^{-1}, while the upper-b counterpart is missing at $V_{\rm LSR} < 0$ km s^{-1}. It is remarkable that the latitude of the missing part of the (b, V) arcs coincides with the latitude where the major disk component is most clearly seen. This can also be recognized in the (l, V) diagrams: The expanding feature at negative $V_{\rm LSR}$ is missing in the (l, V) diagrams at positive latitudes where the major molecular arm (Arm I in Paper I) is most prominent. On the other hand, the feature with positive $V_{\rm LSR}$ is missing at negative latitudes where Arm II is most prominent. Figure 3 shows the relation of the Arms and missing parts of the expanding molecular features. In Paper I, we interpreted that Arms I and II comprise a ring of radius 120 pc around the Galactic Center, and they are located at opposite halves of the ring. The anti-correlation of the expanding shell features with the Arms can be understood if the near side (negative velocity side) of the expanding shell has been interrupted by Arm I, which is in front of the nucleus. On the other hand, the far side of the shell has been interrupted by Arm II, which is on the far side of the nucleus.

Table 1. Dumbbell-shaped expanding molecular shell.*

Radius	1.°2=180 ($\pm$5) pc
Vertical extent	$\sim \pm 50$ pc
Thickness of the shell	$\sim$ 15 pc
Rotation velocity	70 ($\pm$10) km s^{-1}
Expansion velocity	160 ($\pm$5) km s^{-1}
Molecular gas mass	$\sim 0.8 \times 10^7 M_\odot$
Kinetic energy	$\sim 2 \times 10^{54}$ erg

* The distance to the galactic center is taken to be 8.5 kpc.
† 10-keV (1.2×10^8 K) thin hot plasma detected by Koyama et al. (1989).

2.4. *Parameters for the EMS*

The mass of the whole EMS can be obtained by using the wider-area survey of Bally et al. (1988). The ^{13}CO intensity towards $l \sim 1.°2$ is roughly $\sim$ 50 K km s^{-1}. We use a recent value of the ^{12}CO to H_2 conversion factor at the galactic center, 0.92×10^{20} H_2 cm^{-2}/K km s^{-1}(Arimoto et al. 1994), and assumed the ^{12}CO to ^{13}CO temperature ratio to be 6.2 (see Paper I). From the $(V_{\rm LSR}$–$l)$ diagram we calculated the averaged intensity in $-0.°6 \leq b \leq +0.°6$, and estimated the molecular (H_2 + He gas) mass of the EMS as $M \sim 0.8 \times 10^7 M_\odot$. Since the expansion velocity is about 160 km s^{-1}, this leads to a total kinetic energy of expansion of $\sim 2 \times 10^{54}$ erg. Table 1 summarizes the derived parameters for the molecular shell.

2.5. *Comparison with Other Data*

A wider view of the expanding-ring feature can be seen in the low-resolution (l, V) diagram. Two vertically extended ridges at $l = \pm 1.°2$ are also recognized in the low-resolution integrated intensity maps (Bally et al. 1988). In figure 4 we compare this global feature with other data as reproduced from Sofue (1989). Figure 4a is a low-resolution (l, V) diagram of the CO line emission. Figure 4b shows the CO intensities integrated within $-100 \leq V_{\rm LSR} \leq -20$ km s^{-1} for $l \leq 0°$ and $20 \leq V_{\rm LSR} \leq 100$ km s^{-1} for $l > 0°$, respectively, as reproduced from Bally et al. (1988). This map represents 'cross sections' of the tangential parts of the EMS, which comprise vertical spurs. The spur at $l = 1.°2$ is shifted

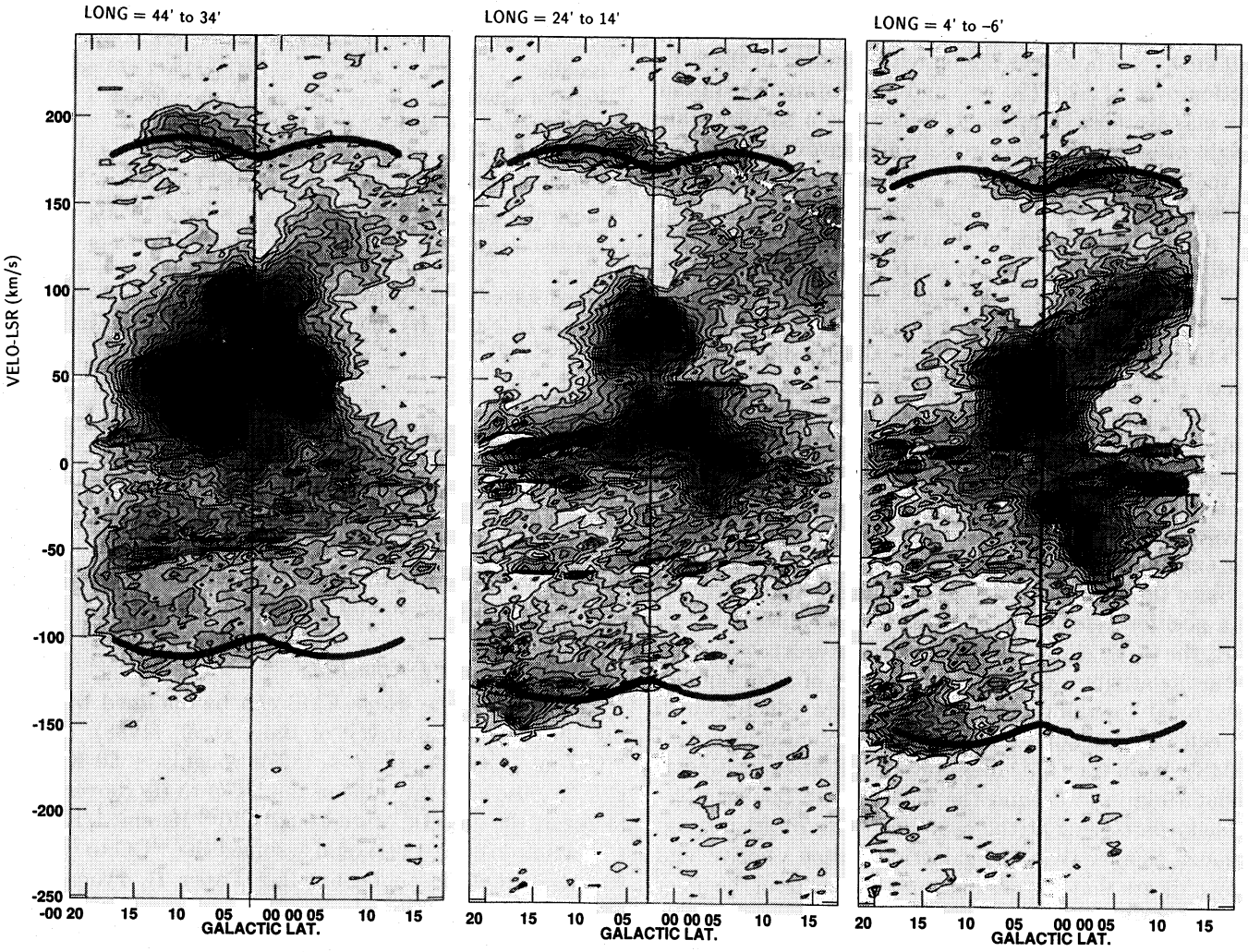

Fig. 2. Typical (b, V) diagrams after subtraction of local/foreground emission. The expanding molecular shell can be fitted by a dumbbell-shape as illustrated by the full lines with its neck (equator) at $b = -3'$. Contours are in unit of K T_A^* at levels $0.1\times(1, 2, 3, ..., 9, 10, 12, 14, 16, 18, 20, 25, 30, 35, 40)$.

toward the positive-latitude side, and can be traced from $b \sim -0.^\circ2$ to $+0.^\circ4$, whereas the spur at $l = -1.^\circ2$ is toward negative latitude, suggesting that the expanding shell is tilted.

Figures 4c to 4e compare the expanding molecular feature with the 10 GHz (Handa et al. 1987) and 2.7 GHz (Reich et al. 1984) radio continuum maps as well as the IRAS 60 μm map (Beichman et al. 1985). Radio continuum maps reveal a number of spurs which emerge from the galactic plane. Near to the tangential direction of the EMS at $l \sim 1.^\circ2$, a spur is visible extending from the galactic plane to ($l = 1.^\circ2$, $b = 0.^\circ4$), which appears to be convex with respect to the Galactic center in a consistent sense with the EMS. The spurs are also identified on the FIR (far-infrared) emission map of IRAS at 60 μm (Beichman et al. 1985), indicating that the EMS contains warm dust. The observed brightness of the thermal radio emission is about 100 mK toward the spur associated with the EMS. If we assume an optically thin ionized gas of $T_e \sim 10^4$ K and $T_B \sim 0.1$ K at $\nu = 10$ GHz, we obtain an emission measure of $EM \sim 4\times10^3$ pc cm^{-6}. We then obtain a thermal-electron density n_e of ~ 6 cm^{-3}, and the total mass of H II gas is derived to be $\sim 4 \times 10^5 M_\odot$ for the same geometry as the EMS. Then, the thermal energy involved in the EMS is on the order of $\sim 10^{51}$ erg.

A hot plasma of $\sim 10^8$ K has been observed in the Galactic center in the iron line at 6.7 keV with the Ginga Satellite (Koyama et al. 1989). The emission region is extended with a size of $1.^\circ8$ (250 pc) about the galactic center, and the observed size of the hot plasma re-

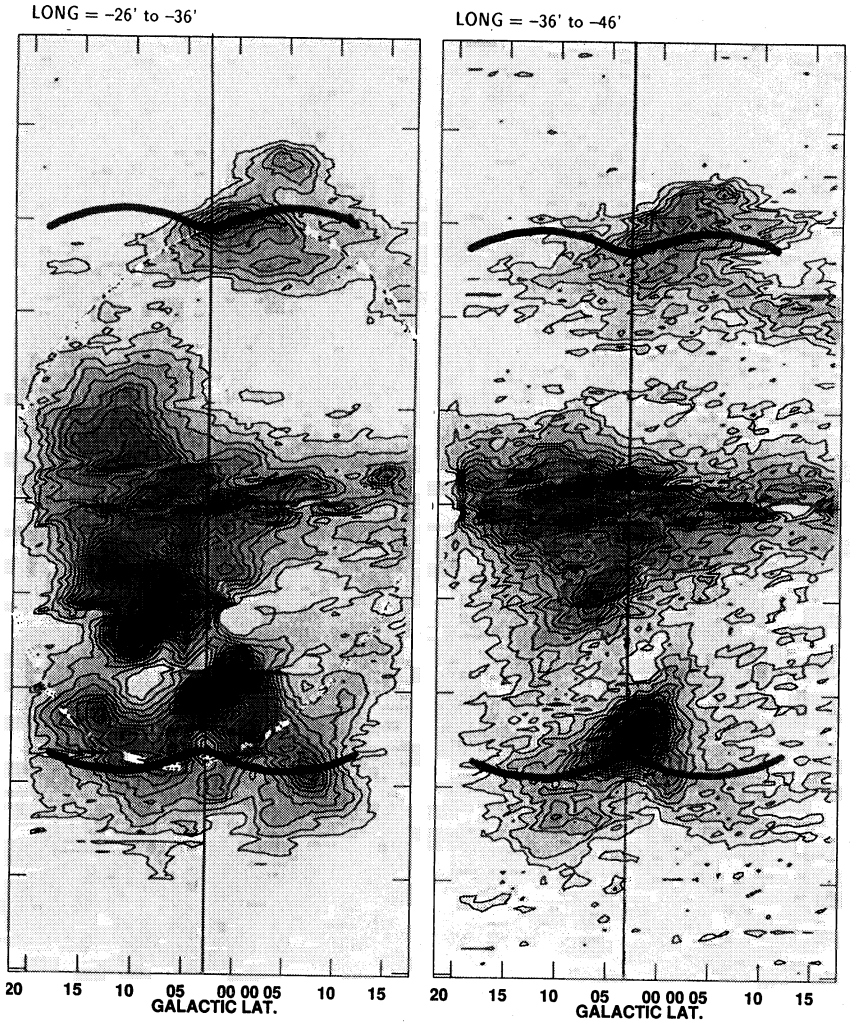

Fig. 2. (continued)

gion fits the interior of the EMS. Considering the angular resolution of the detector and data-sampling grids, we may suggest that the plasma is surrounded by the EMS. However, the time scale of the expansion of the hot plasma ($\sim$ radius/sound velocity $\sim$ 100 pc/1000 km $s^{-1}\sim 10^5$ yr) is much shorter than the expansion time scale of the molecular feature. Therefore, the origin of the hot plasma would not be directly related to the origin of the EMS, but the molecular gas could only act to confine the plasma in the spheroidal, or possibly cylindrical, space. Moreover, the thermal energy contained by the hot plasma ($\sim 3 \times 10^{53}$ erg; Koyama et al. 1989; Sofue 1989) is much smaller than the kinetic energy of the EMS, which implies that the hot plasma cannot be a driving power for the EMS formation.

3. Discussion

We have shown that the so-called expanding molecular ring in the galactic center is a part of a dumbbell-shaped expanding shell with its equator (neck) in the dense molecular disk. The shell is squeezed near its equator, probably due to interruption by the dense disk gas near the galactic plane. The positive latitude and negative-velocity side (near side of the nucleus) of the EMS appears to be interrupted by the near-side Arm I, while the negative-latitude and positive-velocity side (far side) of the EMS is interrupted by the far-side Arm II. These structures suggest that the EMS is an expanding molecular spheroid interacting with the dense molecular disk which comprises the ring and arms.

Figure 5 illustrates the proposed dumbbell-shaped spheroid in $(l, b, V_{\rm LSR})$ space. This may be transposed to

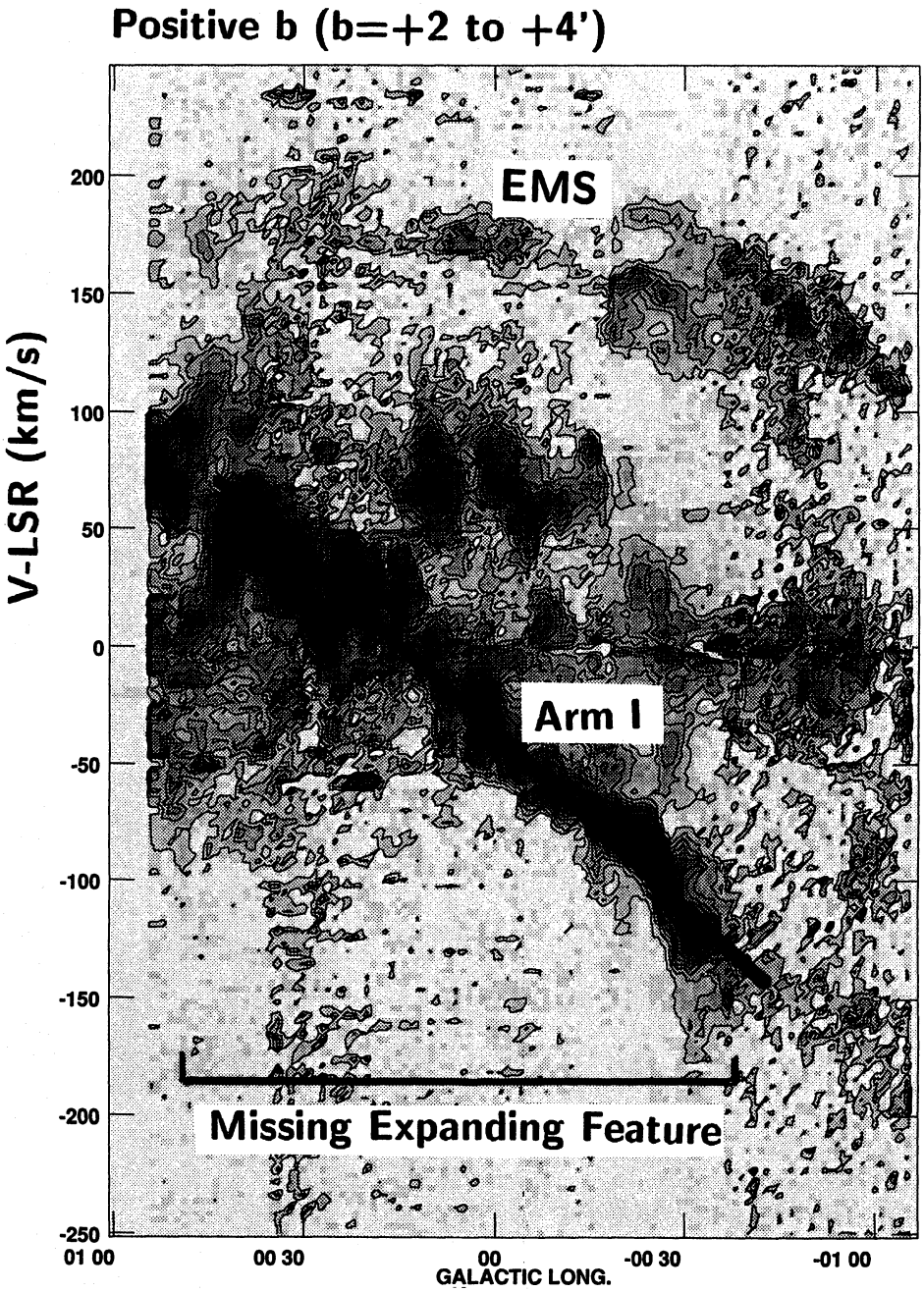

Fig. 3. (l, V) diagrams at $b = +2$ to $+4'$ and at $b = -10$ to $-8'$. This diagrams show an anti-correlation of the disk components Arms I and II with the missing parts of the expanding features at positive and negative latitude sides, respectively.

a three-dimensional expanding spheroid in (x, z, y) space, where x, z, and y are axes along the galactic plane, rotation axis, and depth in the line-of-sight direction, respectively. The expanding molecular gas is observed to be distributed in the intermediate-latitude regions of the spheroid. The gas in the equatorial and polar regions are missing. The asymmetry of the distribution of gas in the EMS with respect to the galactic plane would be somehow related to the fact that the major molecular disk containing Arms I and II is tilted by 5° from the galactic plane.

The total kinetic energy of the shell is approximately 2×10^{54} erg, which is equivalent to the energy released by $\sim 10^3$ type II-SN explosions. It is likely that the

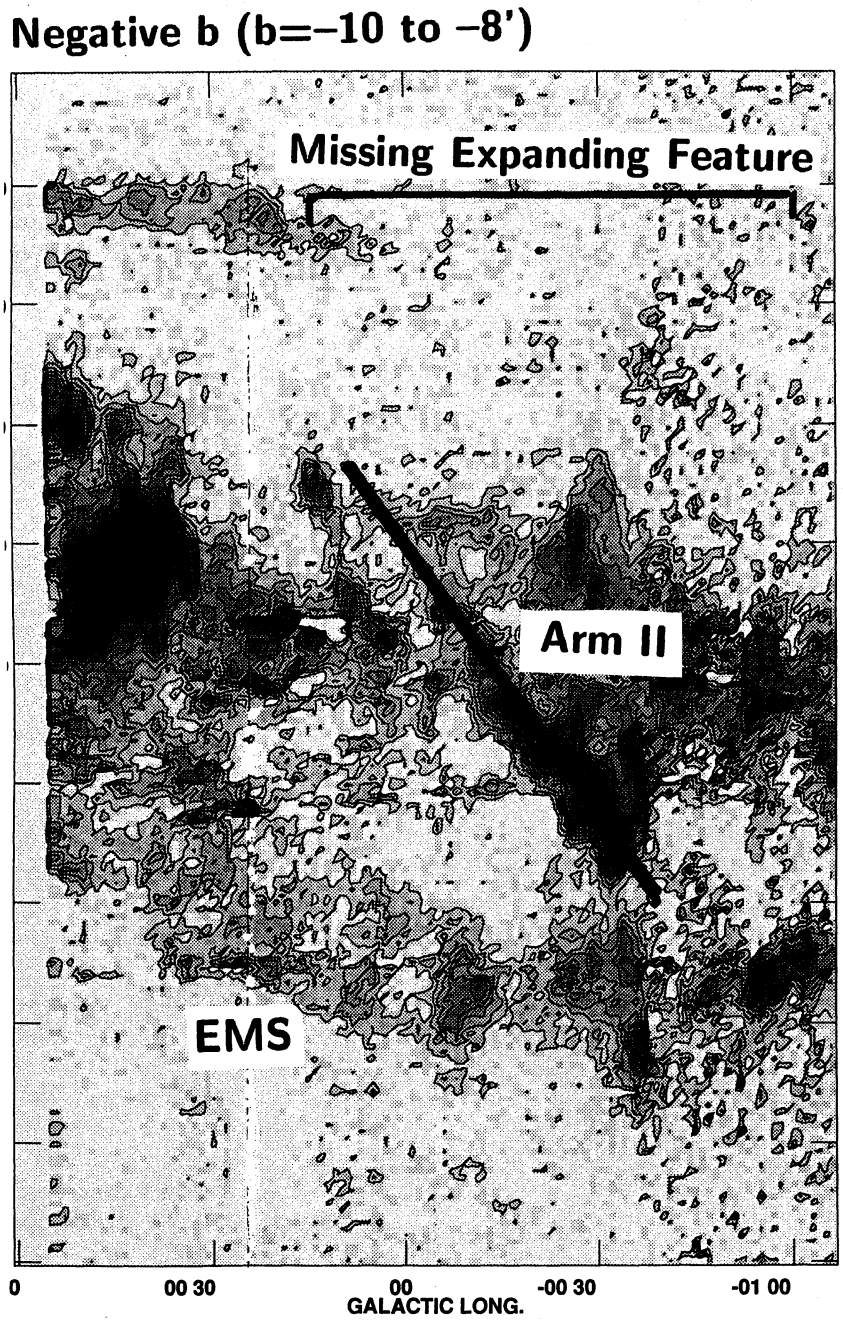

Fig. 3. (continued)

Galactic center experienced a phase of intense star formation in the past $\sim 10^6$ yr. Suppose that coherent star formation containing some 10^3 SN explosions (mini-burst) lasted for a period short enough compared to the EMS's lifetime, e.g., within $\sim 10^5$ yr at the central part of the nuclear disk some 10^6 yr ago. Then, subsequent SN explosions would have formed many shocked shells. Soon after the explosions, the shock fronts would have accumulated on a single large shell expanding into the disk and halo. Such a shocked shell would become deformed by the disk-to-halo density gradient, and would easily attain a dumbbell shape with the neck in the disk plane. Simulations of shock front evolution in a disk-halo system have shown that an initially spherical shocked shell becomes elongated in the direction of the halo, and then attains a dumbbell shape (Sofue 1984, 1994). If the

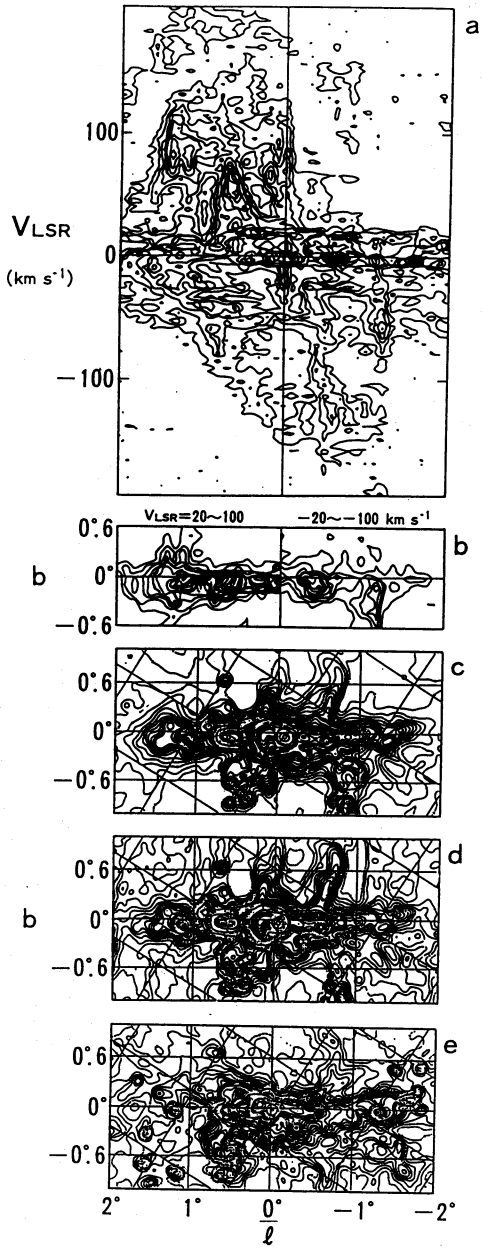

Fig. 4. Comparison in the same scale of ^{13}CO(J = 1–0) data with radio and FIR maps (reproduced from Sofue 1989): (a) The (l, V) diagram of the ^{13}CO gas (reproduced from Bally et al. 1988). (b) CO intensity distribution integrated in the velocity ranges from 20 to 100 km s^{-1} for $l \geq 0°$, and from -20 to -200 km s^{-1} for $l \leq 0°$ (Bally et al. 1988). (c) A radio continuum map at 2.7 GHz (Reich et al. 1984). The background emission of scale sizes greater than 0°.4 has been subtracted, and the map is smoothed to 6′ resolution. (d) The same as (c) but at 10 GHz (Handa et al. 1987). (e) The same as (c) but at 60 μm made from the IRAS data (Beichmann 1985).

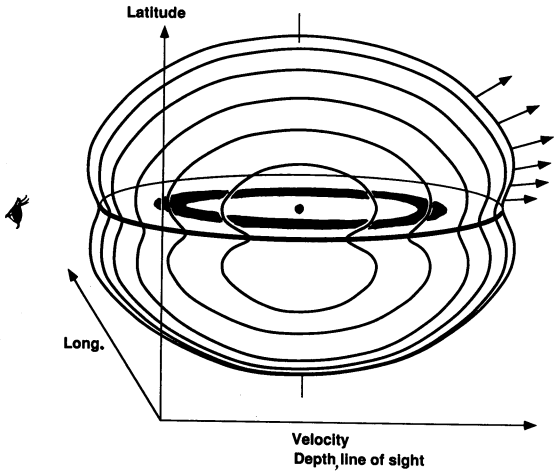

Fig. 5. Schematic view of the dumbbell-shaped shell in $(l, b, V_{\rm LSR})$ space, which may be transposed to a similar shaped three-dimensional expanding spheroid, which is rotating at 70 km s^{-1}and expanding at 160 km s^{-1}. The molecular gas is distributed in the intermediate-latitude regions of the spheroid, and is missing in the equatorial and polar regions.

gravity, which is stronger in the direction perpendicular to the galactic plane, as well as the fact that the disk gas before repulsion was rotating with the centrifugal force, are taken into account, the oblateness of the EMS could be accounted for.

Finally, we comment on another model of the expanding molecular feature. The closed-orbit model based on the "parallelogram" in the (l, V) plot, as proposed by Binney et al. (1991), would be an alternative promising possibility to explain the present expanding molecular features in the (l, V) plot. If the model is successful in reproducing the rigid-rotation features of the disk component, which shares 85% of the mass of the total emission in the (l, V) plot (Paper I) of the presently discussed area, this model would be attractive, since most of the (l, V) features can be understood under a unified theoretical scheme of gas dynamics in a central bar potential. It is also an open question concerning this model, if it can explain the three dimensional structure pointed out in this paper.

The author would like to express his sincere thanks to Dr. John Bally for making himself available along with the molecular line data in a machine-readable format.

References

Arimoto N., Sofue Y., Tsujimoto T. 1994, ApJ submitted

Bally J., Stark A.A., Wilson R.W., Henkel C. 1987, ApJS 65, 13
Bally J., Stark A.A., Wilson R.W., Henkel C. 1988, ApJ 324, 223
Beichman C.A., Neugebauer G., Habing H.J., Clegg P.E., Chester T.J. (ed) 1985, IRAS Explanatory Supplement, JPL D-1855 (Jet Propulsion Laboratory, Pasadena)
Binney J.J., Gerhard O.E., Stark A.A., Bally J., Uchida K.I. 1991, MNRAS 252, 210
Handa T., Sofue Y., Nakai N., Hirabayashi H., Inoue M. 1987, PASJ 39, 709
Kaifu N., Iguchi T., Kato T. 1974, PASJ 26, 117
Kaifu N., Kato T., Iguchi T. 1972, Nature Phys. Sci. 238, 105
Koyama K., Awaki H., Kunieda H., Takano S., Tawara S., Yamanuchi S., Hatsukade I., Nagase F. 1989, Nature 339, 603
Liszt H.S., Burton W.B. 1978, ApJ 226, 790
Reich W., Fürst E., Steffen P., Reif K., Haslam C.G.T. 1984, A&A 58, 197
Scoville N.Z. 1972, ApJL 175, L127
Sofue Y. 1984, PASJ 36, 539
Sofue Y. 1989, Ap. Let. Com. 28, 1
Sofue Y. 1994, ApJL 431, L91
Sofue Y. 1995, PASJ 47, 527 (Paper I)
Sofue Y., Handa T. 1984, Nature 310, 568